China Geology 2 (2021) 230−244

China Geology

Journal homepage: http://chinageology.cgs.cn
https://www.sciencedirect.com/journal/china-geology

Hydrothermal alteration processes in the giant Dahutang tungsten deposit, South China: Implications from litho-geochemistry and mass balance calculation

Hai-Bo Zhao[a, d], Yong Zhang[b, c,*], Lei Liu[a, d]

[a] *Zhengzhou Institute of Multipurpose Utilization of Mineral Resources*, *Chinese Academy of Geological Sciences*, *Zhengzhou* 450006, *China*
[b] *State Key Laboratory of Nuclear Resources and Environment*, *East China University of Technology*, *Nanchang* 330013, *China*
[c] *Institute of Geological Survey of East China University of Technology*, *Nanchang* 330013, *China*
[d] *Northwest China Center for Geoscience Innovation*, *Xi'an* 710054, *China*

ARTICLE INFO

Article history:
Received 15 October 2020
Received in revised form 16 November 2020
Accepted 7 January 2021
Available online 25 January 2021

Keywords:
Tungsten deposit
Geochemistry
Alteration
Mass balance calculation
Hydrothermal circulation
Dahutang
Mineral exploration engineering
Jiangnan Orogenic Belt
South China

ABSTRACT

The giant Dahutang tungsten (W) deposit has a total reserve of more than 1.31 Mt WO_3. Veinlet-disseminated scheelite and vein type wolframite mineralization are developed in this deposit, which are related to Late Mesozoic biotite granite. Four major types of alterations, which include albitization, potassic-alteration, and greisenization, and overprinted silicification developed in contact zone. The mass balance calculate of the four alteration types were used to further understanding of the mineralization process. The fresh porphyritic biotite granite has high Nb, Ta, and W, but low Ca and Sr while the Jiuling granodiorite has high Ca and Sr, but low Nb, Ta, and W concentrations. The altered porphyritic biotite granite indicated that the Nb, Ta, and W were leached out from the fresh porphyritic biotite granite, especially by sodic alteration. The low Ca and Sr contents of the altered Neoproterozoic Jiuling granodiorite indicate that Ca and Sr had been leached out from the fresh granodiorite by the fluid from Mesozoic porphyritic biotite granites. The metal W of the Dahutang deposit was mainly derived from the fluid exsolution from the melt and alteration of W-bearing granites. This study of alteration presents a new hydrothermal circulation model to understand tungsten mineralization in the Dahutang deposit.

1. Introduction

Hydrothermal ore deposits commonly show close relationships with hydrothermal alteration. Thus, alteration is imperative for ore metal mineralization, especially for a granite-related metal deposit. Currently, there are many granite-related ore systems, such as granite-pegmatite, skarn, greisen-veins and porphyry deposits (Sial AN et al., 2011). To establish the granite-related ore systems genetic models cannot avoid the study of ore-forming metal transport and deposition by fluid-rock reactions. Each ore system has a distinctively different alteration process. Porphyry deposits are characterized by several representative alteration assemblages (potassic, propylitic, phyllic, and argillic alteration), and high-grade mineralization typically occurs in the potassic-altered centre of the deposit (Lowell JD and Guilbert JM, 1970; Gustafson LB and Hunt JP, 1975; Sillitoe RH, 1997, 2010). Porphyry mineralization occurs predominately by fluid-rock interaction to form large accumulations of sulphides, and the alteration types of ores. The alteration and evolution processes of porphyry systems are relatively well understood (Kusakabe M, 1984; Kusakabe M et al., 1990; Wolfe R et al., 1996; Corbett GJ and Leach TM, 1998; Watanabe Y and Hedenquist JW, 2001; Harris AC and Golding SD, 2002; Cooke DR, 2005; Seedorff E et al., 2005; Sillitoe RH, 2000; Hou ZQ et al., 2007, 2012; Cooke DR et al., 2014). The most important are the metals accumulated by crustal-scale hydrothermal fluid circulation, which originates from the porphyry/granite system (Weisheit A et al., 2013; Nadeau O, 2015; Plümper O et al., 2017a, 2017b).

However, research on the relationship between tungsten mineralization and alteration type is comparatively weak compared to that of the porphyry systems. Granite-related tungsten deposits host more than 99% tungsten resource in the world, characterized by various types of alteration zones due to granite intrusion, and almost spatially associated with

First author: *E-mail address*: tiger_zhaohb@163.com (Hai-Bo Zhao).
* Corresponding author: *E-mail address*: zhycy2004@163.com (Yong Zhang).

doi:10.31035/cg2021003
2096-5192/© 2021 China Geology Editorial Office.

greisenization, and silicification (Mao JW et al., 1996; Hu SX et al., 2004; Pirajno F, 2013; Soloviev SG and Kryazhev S, 2016, 2017; Wang H et al., 2016; Soloviev SG and Kryazhev S, 2017). The fluid-rock interaction is decisive for the formation of tungsten deposits (Lecumberri-Sanchez P et al., 2017). Such fluid-rock interactions are direct records of the alteration rocks at the tungsten deposit.

The Dahutang W deposit is exceptional is one of a few giant tungsten deposits, with a reserve of more than 1.31 Mt WO_3 (with an average grade of 0.03%), 0.78 Mt Cu (with an average grade of 0.06%), and 0.06 Mt Mo (with an average grade of 0.01%). The ratio of scheelite to wolframite is approximately 1.0 (Zhang Y et al., 2018a). This deposit has comprehensive, complicated alteration zones characterized by a large area (approximately 10×15 km^2) of alkaline alteration, overprinted locally by acidic alteration. The alkaline alterations have different characteristics in the Mesozoic porphyritic biotite granite and Jiuling Neoproterozoic granodiorite.

Tungsten mineralization in the Dahutang deposit is spatially related to the Cretaceous porphyritic biotite granite and fine-grained biotite granite. Drill records show that tungsten mineralization occurs at the contact zone between the Late Mesozoic granite stocks (about 150 Ma; Mao ZH et al., 2015) and the Jiuling Neoproterozoic granodiorite batholith (about 820 Ma; Zhong YF et al., 2005; Li XH et al., 2003) or the Neoproterozoic slate. A majority of the known work on the Dahutang tungsten deposit focused on the petrogenetic and metallogenic geochronology and obtain many important and meaningful research results (Mao ZH et al., 2013; Huang LC and Jiang SY, 2013, 2014; Xiang XK et al., 2013a; Jiang SY et al., 2015; Zhang ZY et al., 2015b; Zhang Y et al., 2015a, 2017; Zhang MY et al., 2016a).

Trace elements and Sr-Nd isotopes of scheelite from the Shimengsi segment in the Dahutang deposit indicate that tungsten was derived from the ore-forming fluids exsolved from the granitic melt (Sun KK and Chen B, 2017). Nevertheless, Li isotopic data suggests that extensive W, Sn, and Cu may be derived from fluids exclusively from the activity of coeval metamorphic fluids and/or high temperature circulating fluids around the granite pluton (Chen B et al., 2018). *In situ* oxygen isotope and trace element characteristic of quartz and mica from the Dahutang deposit not only traces the processes of W enrichment by magmatic differentiation but also traces the leaching of W by the hydrothermal fluids (Zhang ZY et al., 2019; Yin R et al., 2019). The origin of the ore-forming fluids is controversial.

In addition, the principal in alteration and fluid composition-related processes of the Dahutang W deposit need to be examined (Zhang Y et al., 2018a). The source of different type of alteration contributing to tungsten mineralization is not clear. While the mechanism of tungsten enrichment and mineralization were granites crystallization differentiation or hydrothermal fluid circulation is unclear. The delicate alteration process and has prevented a good understanding of the genesis of the giant W deposit due to the intrusion of the Late Mesozoic granite system. Therefore, a new model for understanding the ore-forming process of the Dahutang W deposit is proposed, to theorize a new perspective to understand this giant tungsten deposit.

In this study, the geology and litho-geochemistry of the Cretaceous porphyritic biotite granite of the Dahutang tungsten deposit is described. The gain/loss ore-forming element, especially Ca, Sr, Nb, Ta, and W, during the alteration processes of fresh/altered hand specimens is examined in detail. These studies are used to develop a genetic model for the Dahutang W deposit.

2. Geological background

2.1. Jiangnan Orogenic Belt

The Jiangnan Orogenic Belt is adjacent to the boundary between the Cathaysia Block and the Yangtze Craton (Mao JW et al., 2006, 2011; Pan YM and Dong P, 1999) (Fig. 1), and is one of the important polymetallic/metallogenic belts in China.

The Shuangqiaoshan Group is an important stratigraphic unit in this belt; it is a Neoproterozoic, low-grade sedimentary stratum approximately 880 Ma (Wang XL et al., 2008b). The Jiangnan orogenic belt experienced multiple orogeneses from the Middle Proterozoic to the Mesozoic (Xu XB et al., 2009; Liu YY et al., 2012; Zhang YQ et al., 2012; Zhang Y et al., 2018a).

Many porphyry-skarn, porphyry-epithermal, skarns/Kiruna style, tin-tungsten, and hydrothermal gold deposits are related to Indosinian-Yanshanian magmatism in the Jiangnan Orogenic Belt (Zaw K et al., 2007). The most significant tungsten deposit is the giant Zhuxi, giant skarn scheelite deposits (Chen GH et al., 2012; Liu SB et al., 2017a). The Xianglushan is another scheelite skarn deposit (Zhang JJ et al., 2008; Xiong X et al., 2015; Fig. 1).

2.2. Jiuling Area

Neoproterozoic granitoids are present in the Jiuling batholith. The Neoproterozoic Jiuling granodiorite intrusion is the largest composite granitoid complex (approximately 820 Ma) in south-eastern China (Fig. 1), intruding into the Shuangqiaoshan Group (Li XH et al., 2003; Zhong YF et al., 2005). The Huashandong tungsten deposit formed 805 ± 5 Ma (Re-Os isochron age) (Liu JX et al., 2015), and may correspond to the Jiuling granodiorite intrusive event. The batholith is a biotite-rich, cordierite-bearing granodiorite. Granodiorite is the dominant rock type and comprises approximately 99% outcrops of the batholith.

The Early Yanshanian tectonic event commenced during the late Middle Jurassic, resulting in the formation of an approximately 1300 km wide, NE-NNE-trending fold-and-thrust system in South China (Xu XB et al., 2009). Cretaceous granitic rocks in the study area are present as multiple small stocks that intruded into both the Neoproterozoic granodiorite batholith and Precambrian strata (Mao ZH et al., 2013) (Figs. 2,3). The granodiorite porphyry was formed about 170–160 Ma (Ding X et al., 2005; Lou FS et al., 2005; Hu ZH et al., 2015). The S-type porphyritic biotite granites formed approximately 150 Ma (Liu J et al., 2008; Huang LC and Jiang SY, 2014; Li Y et al., 2014; Jia LQ et al., 2015b; Mao

ZH et al., 2015; Zhang MY et al., 2016a). Most of the S-type fine-grained biotite granites formed approximately 144 Ma (Ding X et al., 2005; Lou FS et al., 2005; Huang LC and Jiang SY, 2014; Mao ZH et al., 2015; Jia LQ et al., 2015a), and intruded into the porphyritic biotite granites, although there were also some intrusions were emplaced into the Neoproterozoic granodiorite batholith. The porphyritic granite and granite porphyry are granite emplaced at approximately 130 Ma (Ding X et al., 2005; Lou FS et al., 2005; Huang LC and Jiang SY, 2014).

2.3. Geologic characteristics of the Dahutang tungsten deposit

The Dahutang deposit is composed of four segments, Shimensi, Dawutang, Shiweidong, and Kunshan (Fig. 2), situated in Wuning County of Jiangxi Province, approximately 120 km NW of Nanchang (Zhang Y et al., 2018a). The Shuangqiaoshan Group was intruded by the Jiuling granitic batholith of granodiorite (Fig. 2). Both the Shuangqiaoshan Group and the Jiuling granodiorite were intruded by a Cretaceous granite series, including the porphyritic biotite granite (151.7 ± 1.3 Ma to 147.4 ± 0.58 Ma) and the fine-grained biotite granite (146.1 ± 0.64 Ma to 144.7 ± 0.47 Ma) (Jiang SY et al., 2015; Mao ZH et al., 2013; Xiang XK et al., 2013a; Huang LC and Jiang SY, 2014; Mao ZH et al., 2015; Zhang MY et al., 2016a; Zhang Y et al., 2018a; Fig. 3).

The mineralized and altered stock of the Dahutang area is part of a surface outcrop of approximately 20 km^2 (Fig. 2) and is elongated within a 10 km long N-NE-trending corridor and consists compositionally of three different granite-style intrusive phases. The spatial relationship of the concessions of all four representative segments can be see directly in a sectional view (Fig. 3).

Fig. 3 shows that the Dahutang deposit has two mineralization ages, but the main mineralization age is approximately 144 Ma. Only the Shimengsi segment has molybdenite Re-Os isochron ages of 139.18 ± 0.97 Ma (Mao ZH et al. 2013), 143.7 ± 1.2 Ma (Mao ZH et al. 2013), 143.7 ± 1.2 Ma (Feng CY et al., 2012), and 149.6 ± 1.2 Ma (Xiang XK et al., 2013a). The Dawutang segment has a Re-Os isochron molybdenite age of 137.9 ± 2.0 Ma (Zhang Y et al., 2017). The Shiweidong segment has a Re-Os isochron molybdenite age of 140.9 ± 3.6 Ma (Feng CY et al., 2012). The Kunshan segment has a Re-Os isochron molybdenite age of 151.0 ± 1.3 Ma (Zhang MY et al., 2016a). These mineralization ages correspond to two Cretaceous granites, the porphyritic biotite granite (approximately 150 Ma) and the fine-grained biotite granite (approximately 144 Ma). The mineralization in the Dahutang tungsten deposit is characterized by: (1) Disseminated veinlet-type tungsten deposits (approximately 95% of the total reserve) that are associated with the porphyritic intrusion (Figs. 2b, 3), (2) the occurrence of wolframite, scheelite, chalcopyrite, and molybdenite hydrothermal crypto-explosive breccia ores (about 4%), and (3) wolframite-scheelite quartz veins and stockworks (about 1%) (Fig. 3).

The Dahutang tungsten deposit is a mostly disseminated-/veinlet-type tungsten mineralization where scheelite and wolframite co-exist and their ratios are approximately equal. Wolframite and scheelite are wrapped and disseminated with each other at the Dahutang W deposit. The mineral impurities of wolframite and scheelite are ubiquitously distributed in the disseminated veinlet-type tungsten deposits (Figs. 4k, l), and are identical at the quartz vein deposit. This character of

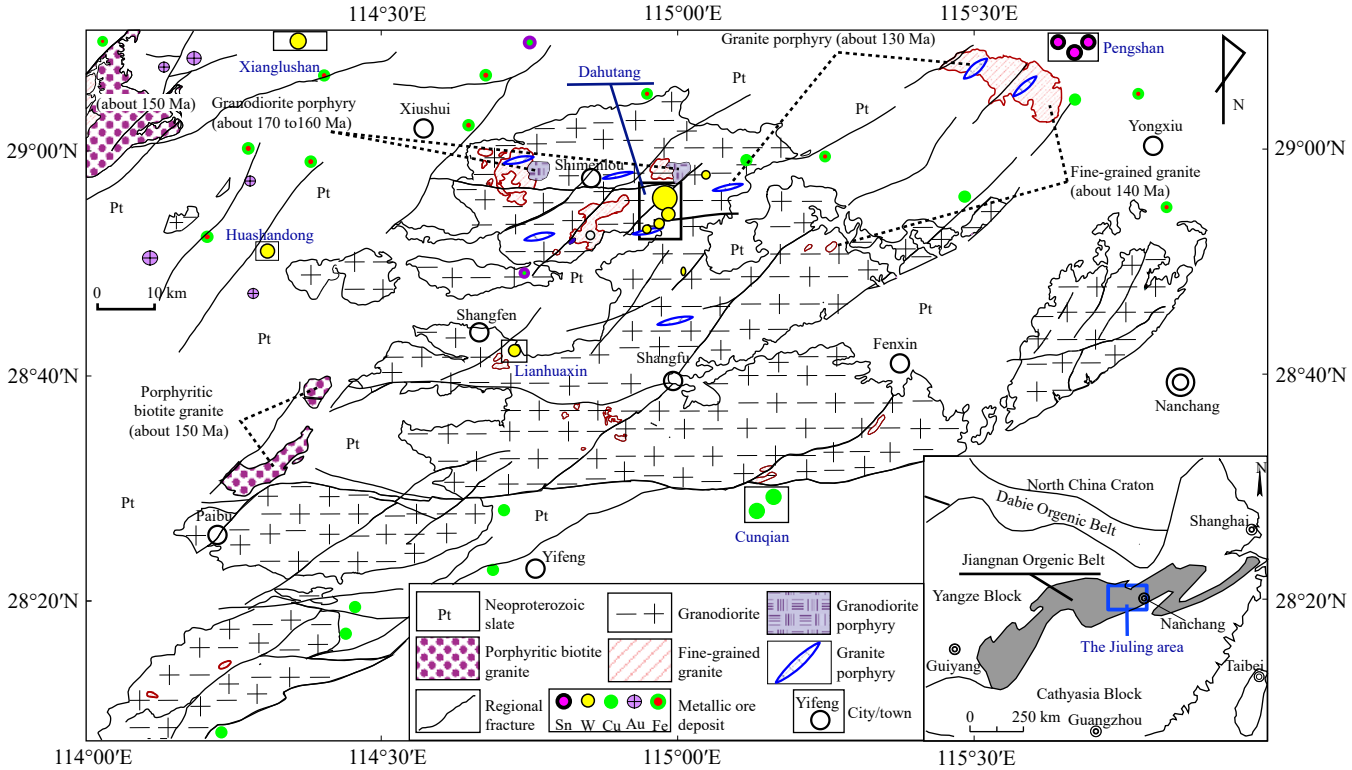

Fig. 1. Schematic geological map and granite-related metal deposit of the Jiuling area (after Li XH et al., 2003; Yang MG et al., 2004; Zhong YF et al., 2005; Wang XL et al., 2008b; Zhang Y et al., 2018a).

mineral impurities also restricts the mineral separation required to implement industrial production.

The most intensely mineralized zone occurs within an 800 m wide cone in the Shimengsi segment with reserves of more than 0.74 MT WO_3 (Xiang XK et al., 2013b), where the Cretaceous porphyritic biotite granite is surrounded by granodiorite, which forms a large biotization + greisenization ± silicification alteration halo (Figs. 2, 3). This is surrounded by a semi-round circumnuclear intrusive dome (roof) of the porphyritic biotite granite, of approximately 500 m radius and a vertical height of 250 m. The tungsten mineralization is mostly concentrated on the alteration superposed zone as the biotization + silicification altered granodiorite. The alteration superposed zone centre is a disseminated veinlet-type cut by quartz veins, spatially to the dome of the porphyritic biotite granite.

The mineralized granodiorite of the Dawutang segment is spatially analogous to the superposed altered dome of the porphyritic biotite granite with hydrothermal crypto-explosive breccia, like the Shimensi segment (Zhang Y et al., 2018a). The Dawutang segment is a recently discovered and currently explored tungsten depsoit, with reserves of more than 0.25 Mt WO_3 (Zhang Y et al., 2017), and has alteration and tungsten mineralization similar to the Shimensi segment (Zhang Y et al., 2018a; Fig. 2). The intrusion in the Dawutang segment has a core of porphyritic biotite granite, which is cut off by fine-grained granite, and later cut by granite porphyry (Zhang Y et al., 2018a).

The Shiweidong segment with reserves of 0.31 Mt of WO_3 (Jiang SY et al., 2015) consisting of large quartz veins (30–100 cm width) and disseminated veinlets (several meters along the quartz vein) in the upper part, with quartz, wolframite, scheelite, molybdenite, chalcopyrite, bornite, and pyrite assemblages (Zhang Y et al., 2018a). The density of the

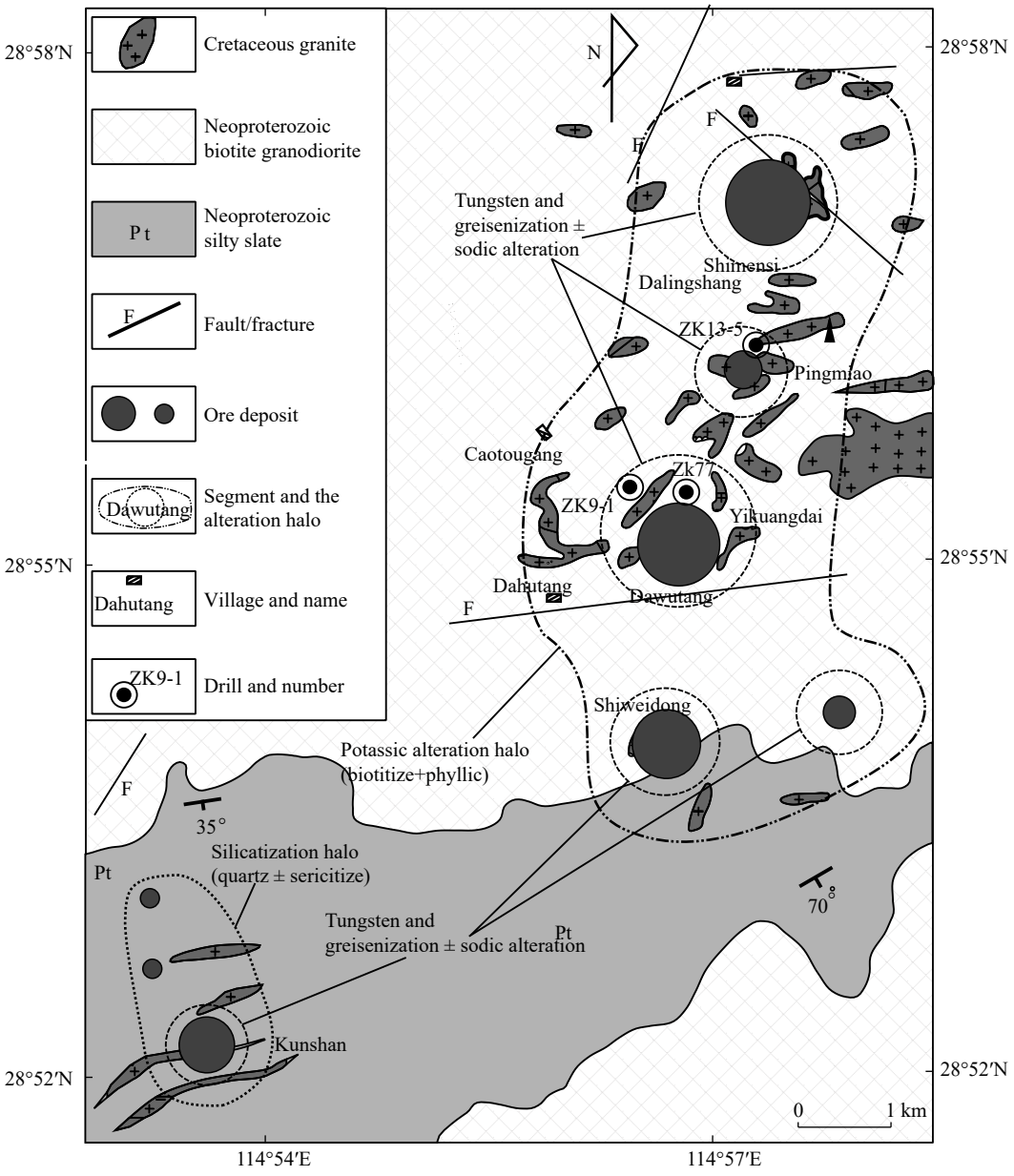

Fig. 2. Schematic geological map of the Dahutang tungsten deposit and Shimensi, Dawutang, Shiweidong, and Kunshan deposits, and their mining boundary (modified from Zhang Y et al., 2018a).

disseminated veinlets system is less than approximately 20–30/m, while the veinlet range is from 1–10 mm in width (Zhang Y et al., 2018a). The phyllic + greisenization altered halo of the external contact zone in the Shiweidong segment formed from the Cretaceous porphyritic biotite granite intruded into the granodiorite and the intrusion contact interface of the granodiorite to the Shuangqiaoshan Group. The granodiorite having intruded into the Shuangqiaoshan Group and exposure half of the surface area at the Shiweidong segment (Zhang Y et al., 2018a). Cretaceous porphyritic biotite granite could only be found in the audit but did not occur at the surface (Zhang Y et al., 2018a).

3. Sampling and analytical methods

3.1. Sampling

Sampling location, host lithology, and type of altered rock are available in the Supplementary material. Four drill cores for the Dahutang tungsten deposit were logged and sampled. The unaltered porphyritic biotite granite samples were obtained from the elevation (610.5 m to 676.5 m) lower than the elevation containing altered samples (764.2 m to 1546.2 m) and far away from ore body at the Dawutang segments. All samples, nearly from 0.5–1.0 kg in size, were collected for more than 300 specimens from localities near the ore deposits and the ores were located in the Shimengsi, Dawutang, Shimeidong, and Kunshan districts. A representative sample selected for detailed analysis consisted of 150 thin sections and 40 major and trace element analyses of the whole rock sample. Those select unaltered and altered porphyritic biotite granite samples from drill holes were located at the Dawutang segment, at ZK9-1 (E 114°56′30″, N28°55′31″; elevation: 1632.46 m), ZK77 (E114°56′39″, N 28°55′33″; elevation: 1598.45 m), and ZK13-5 (E114°57′23″, N 28°56′26″; elevation: 1564.77 m).

3.2. Analytical methods

All the bulk samples were analysed at the Analytical Laboratory Beijing Research Institute of Uranium Geology. The major elements were analysed using X-ray fluorescence spectrometry (XRF) (Zhang FX et al., 2009); ferric and ferrous iron measurements were determined by wet chemical analyses (titration). The analytical precision for major oxides, which is based on certified standards (GSR-1, GSR-3) and duplicate analyses, were expressed in terms of relative percentages and ranges from ± 0.01% to ± 0.20%. The trace elements were determined using the inductively coupled plasma mass spectrometry (ICP-MS) solution at the

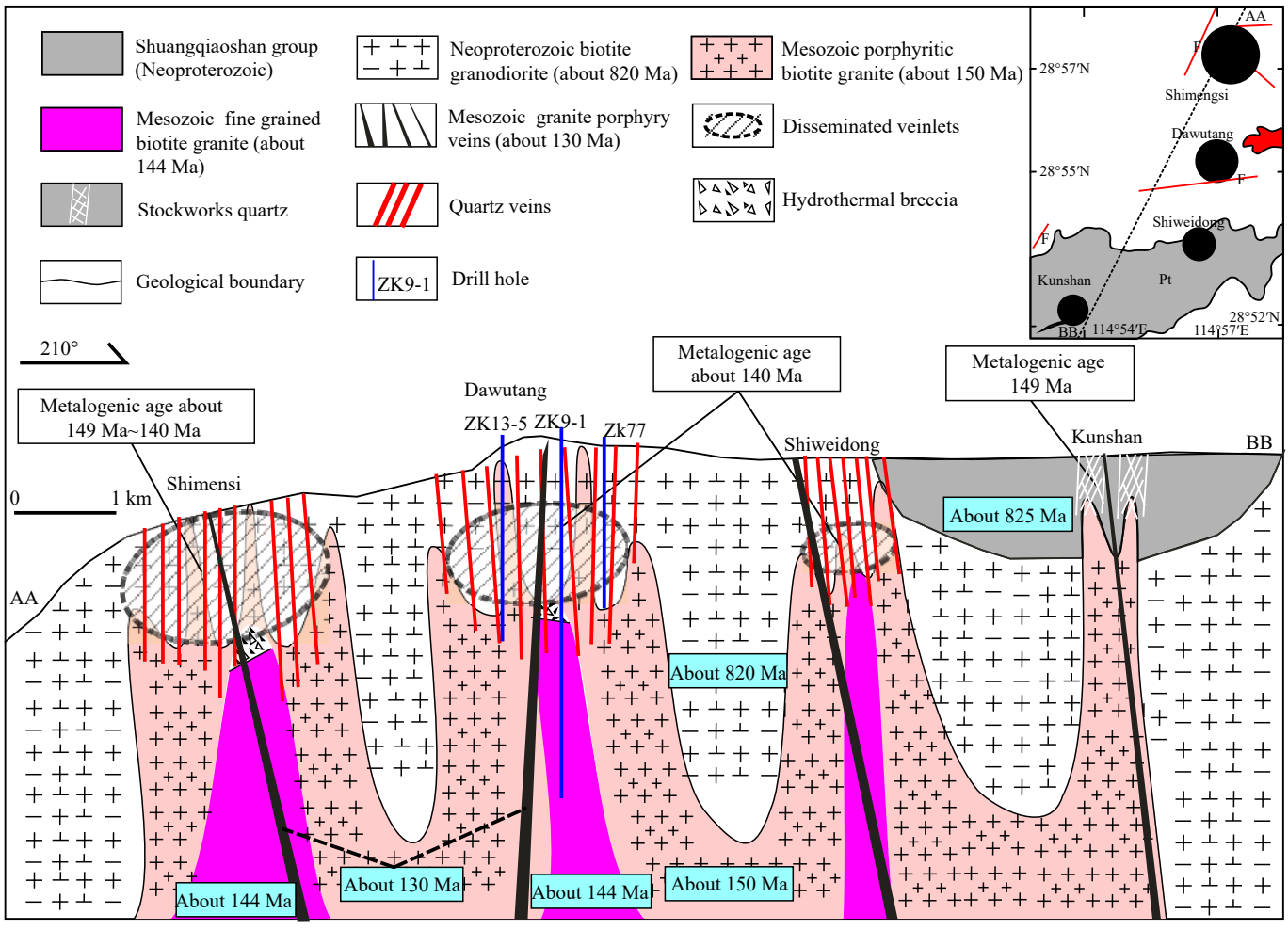

Fig. 3. Diagrammatic sketch of the alteration halo for the representative deposits of the Dahutang tungsten deposit (modified from Zhang Y et al., 2018a).

Analytical Laboratory Beijing Research Institute of Uranium Geology. Approximately 50 mg rock powders were weighed and dissolved in a mixture of distilled HF and 0.5 mL of HNO_3 (1.41 g/mL) in a Teflon-lined stainless, sealed bomb. The sealed bombs were then placed in an oven and heated to 190℃ for 24 h. After cooling, the bombs were opened and placed on a hotplate for evaporation at 60°C to dryness. The residue was dissolved using a 30% HNO_3 solution, resealed and heated at 130°C for 3 h. The final solutions were transferred into plastic beakers and diluted prior to the analysis. The detailed sample preparation methods, instrument operating conditions and calibration procedures were followed based on Liang Q and Grégoire DC (2000) and Gao JF et al. (2003). Two standards (granite GSR-1 and basalt GSR-3) were used to monitor the analytical quality of the data.

4. Result

4.1. Petrography of porphyritic biotite granite

4.1.1. Unaltered porphyritic biotite granite

The Cretaceous granites are compositionally and structurally categorized as porphyritic biotite granite, fine-

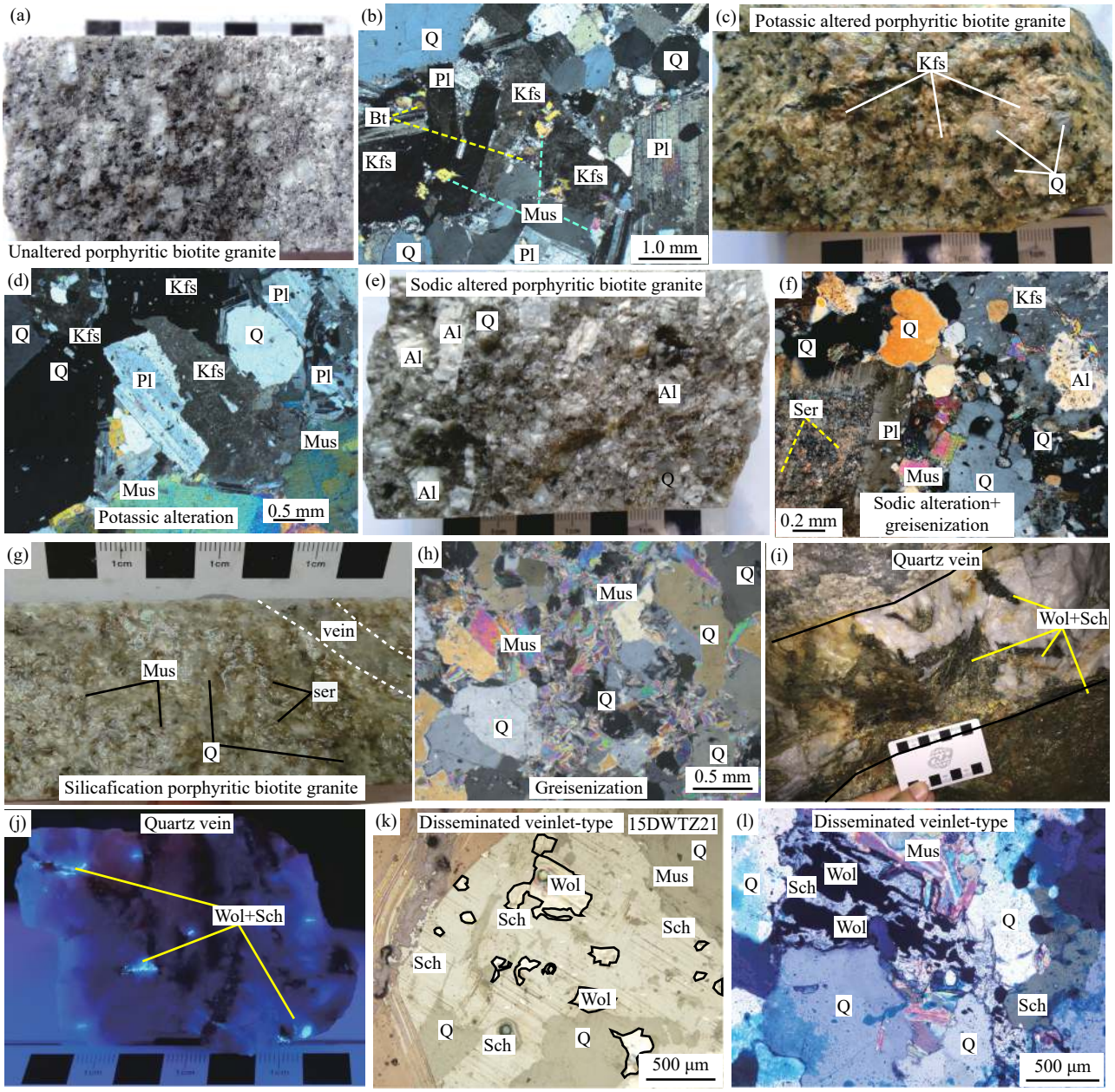

Fig. 4. Photomicrographs in transmitted light of the unaltered and altered porphyritic biotite granite and the ore mineral assemblage. a–unaltered porphyritic biotite granite specimen. b–transmitted light of the unaltered porphyritic biotite granite, and its distinct mineral grain boundaries. c–potassic porphyritic biotite granite. d–transmitted light of the potassic porphyritic biotite granite, and the K-feldspar alter the plagioclase. e–sodic porphyritic biotite granite specimen. f–transmitted light of the sodic porphyritic biotite granite, the albite altered K-feldspar, and the sericite altered plagioclase. g–greisenization porphyritic biotite granite. h–transmitted light of the greisenization porphyritic biotite granite. i, j–wolframite and scheelite quartz veins. k, l–disseminated veinlet-type tungsten deposits. Qz–quartz, Pl–plagioclase, Kfs–K-feldspar, Bt–biotite, Mus–muscovite, Ccp–chalcopyrite, Wol–Wolframite, Sch–Scheelite.

grained granite, coarse-grained biotite granite, and granite porphyry dikes. The porphyritic biotite granite is the most abundant and it is cut by subordinate fine-grained granite; coarse-grained granite is the central phase of the fine-grained granite, mostly seen deep of the drillcore just below the fine-grained granite. The granite porphyry dikes are younger than both the porphyritic biotite granite and fine-grained granite (Mao ZH et al., 2015).

The unaltered porphyritic biotite granite is grey to white in colour (Figs. 4a, b), with up to approximately 35%–50% modal percent phenocrysts. The phenocrysts are approximately 35%–40% in volume, 1–3 mm in diameter; approximately 35% K-feldspar, 0.5–4 mm in diameter; approximately 10%–15% plagioclase; and 10% biotite in a fine-grained matrix (Zhang Y et al., 2018a). The matrix is composed of quartz, K-feldspar, plagioclase, and biotite. The phenocrysts are multiple metasomatic altered by the hydrothermal fluid, thereby displaying jagged edges and a sieve-like texture (Zhang Y et al., 2018a). The major accessory minerals include apatite, zircon, garnet, ilmenite, magnetite, monazite, epidote, tetrahedrite, and arsenopyrite (Zhang Y et al., 2018a).

4.1.2. Alteration types of the porphyritic biotite granite

Four alteration types have been identified for the Dahutang deep alteration zone in the porphyritic biotite granite. Type I: Sodic alteration comprised of albitization/microclinite (Figs. 4e, f); Type Ⅱ: Potassic alteration comprised of K-feldspar (Figs. 4c, d); Type Ⅲ: Greisenization, the weak alkaline hydrothermal alteration, mostly muscovite and some quartz (Figs. 4g, h), that occurred following the potassic and sodic alteration, as the mineral deposition began with some wolframite ± scheelite; Type Ⅳ: Silicification (Fig. 4l) comprised of muscovite ± quartz + wolframite + scheelite ± sulphide.

(i) Sodic alteration (perthites ± albitization). Sodic alteration is the first alkaline alteration at the lowest elevation of all four-alteration types. It is characterized by Na-bearing minerals (perthites, albite, and paragonites), which show replacement relationships with the primary magmatic minerals. The replacement of alkaline feldspar by albite (albitization or Na-feldspathization) is the common form of sodic alteration (Figs. 4e, f). This replacement may proceed from pre-existing perthites, or by direct replacement of K-feldspar with newly formed albites.

(ii) Potassic alteration (K-feldspar ± muscovite). The potassic alteration occurred after the sodic alteration and is characterized by a secondary K-feldspar (perthite), mostly in the Neoproterozoic granite. In addition, secondary biotite grains, mostly in the porphyritic biotite granite can be found in this formation (Figs. 4c, d). Moreover, most of the formed biotite are dark and small, many are 0.1–1.0 mm, in hand specimen. The potassic alteration manifested by the replacement of pre-existing phenocrysts within ground mass or crystallization of secondary veinlets in the Jiuling biotite granodiorite. A secondary biotite, K-feldspar, muscovite, sericite, chlorite, ilmenite, chalcopyrite, pyrite, molybdenite, and magnetite assemblage represents this alteration. Secondary K-feldspar occurs as a replacement for plagioclase and quartz phenocrysts (Figs. 4c, d).

(iii) Greisenization (muscovite ± quartz). Greisenization is a potassic alteration that differs from a traditional definition. A zone of mostly muscovite and some quartz is close to muscovitization (Hu SX et al., 2004; Pirajno F, 2013), which developed at the depth of the porphyritic biotite granite far from the roof zone at Dawutang. The muscovites from the greisen sample are mostly Li-phengite and zinnwaldite as determined by an electron probe microanalysis. The greisenization was overprint by later silicification events (Figs. 4f, g). The greisenization is characterized by the replacement of most of the rock-forming silicates such as plagioclase, biotite, and amphibole by muscovite + quartz, but some are accompanied by variable amounts of sericite, chalcopyrite, and pyrite. These alterations have resulted in a colour change of the rock surface from relatively dark grey to light grey and light green.

(iv) Silicification (quartz ± muscovite). Silicification is at the highest elevation, spatially, of the tungsten mineralization, and close to the upper superposition, in the biotization + greisenization altered Jiuling biotite granodiorite, the main ore (Zhang Y et al., 2018a). The silicification overprints not only the core biotite but also the peripheral greisenization alteration zones and forms a halo around the mineralized biotite or sericite zone, mostly showing a reduction in biotite and feldspar (Figs. 4e, h). It is characterized by the occurrence of secondary quartz, muscovite, wolframite, scheelite, chalcopyrite, molybdenite, and pyrite. These alteration minerals are formed most commonly by the replacement of primary and secondary minerals as the hydrothermal fluid permeates the geologic body. Primary and secondary biotite phenocrysts partially alter to become muscovite or sericite.

4.2. Whole rock geochemistry of porphyritic biotite granite

4.2.1. Unaltered porphyritic biotite granite

The unaltered porphyritic biotite granite samples have characteristically high SiO_2 content measured as fraction by weight (72.17%–73.61%, average 72.66%), Na_2O (3.58%–4.31%, average 3.82%), and K_2O (3.76%–5.46%, average 4.77%). While there are characterized by low TiO_2 (0.05%–0.14%, average 0.11%), Al_2O_3 (14.35%–14.91%, average 14.65%), Fe_2O_3 (0.26%–0.43%, average 0.38%), MnO (0.05%–0.07%, average 0.06%), MgO (0.11%–0.26%, average 0.21%). Moreover, the unaltered porphyritic biotite granite samples are characterization of low CaO (0.40%–0.71%, average 0.58%), P_2O_5 (0. 25%–0. 30%, average 0.28%), FeO (1.78%–2.22%, average 1.89%). (see Supplementary Table S1)

The trace elements from the porphyritic biotite granite samples had high W content (average 1020×10^{-6}), Nb (21.36×10^{-6}), Ta (13.41×10^{-6}) (Table S1). In particular, low Sr (average 32.06×10^{-6}) content indicates a slightly non-fluid rock reaction, as the initial host-rock composition is unaltered porphyritic biotite granite.

4.2.2. Altered porphyritic biotite granite

Samples with sodic alteration have characteristically

lower SiO_2 content (63.10%–67.86%, average 65.48%), FeO (1.99%–2.04%, average 2.02%), and K_2O (2.26%–2.57%, average 2.42%) content compared to those of the fresh rocks (the unaltered porphyritic biotite granite; Table S1). They had higher Al_2O_3 (17.17%–20.95%, average 19.06%), Fe_2O_3 (0.29%–0.52%, average 0.41%), MgO (0.42%–0.45%, average 0.81%), CaO (1.09%–1.38%, average 1.20%), Na_2O (6.17%–7.69%, average 5.98%), and P_2O_5 (0.19%–0.74%, average 0.82%) content compared to those of the fresh rocks. The samples are enriched in most trace elements Sr (111.00×10^{-6}–166.00×10^{-6}, average 138.50×10^{-6}), compared to the fresh samples, but obviously depleted in W (12.2×10^{-6}–29.9×10^{-6}, average 21.05×10^{-6}), and Nb (11.3×10^{-6}–16.3×10^{-6}, average 13.80×10^{-6}), and Ta (2.75×10^{-6}–5.94×10^{-6}, average 4.35×10^{-6}).

In addition, samples with potassic alteration have lower SiO_2 (54.94%–66.00%, average 60.47%) and Na_2O (0.25%–0.34%, average 0.30%) content; however, the have higher Al_2O_3 (18.23%–25.16%, average 21.72%), Fe_2O_3 (0.68%–1.05%, average 0.86%), MgO (0.81%–0.89%, average 0.85%), CaO (1.20%–1.28%, average 1.24%), K_2O (5.98%–7.84%, average 6.91%), and P_2O_5 (0.61%–0.82%, average 0.72%) content (Table S1). Those samples are enriched in the trace elements Sr compared to fresh samples, while gradually deplete W (94.90×10^{-6}), Nb (16.40×10^{-6}), and Ta (8.13×10^{-6}).

While samples with greisenization present low content of SiO_2 measured as fraction by weight (average 71.37%), Al_2O_3 (average 14.22%), and Na_2O (average 1.85%) content and higher Fe_2O_3 (average 0.53%), MgO (average 0.42%), CaO (average 1.05%), K_2O (average 5.03%), P_2O_5 (average 0.23%), and FeO (average 3.12%) compared to that of the fresh rocks (Table S1). They were enriched in the elements Sr (average 88.78×10^{-6}), nevertheless gradually depleted in W (average 326×10^{-6}), Nb (average 12.67×10^{-6}), and Ta (average 1.77×10^{-6}) compared to the fresh rock.

Finally, samples with silicification display obviously low: Al_2O_3 (average 12.03%), Na_2O (average 3.08%), K_2O (average 3.25%), and P_2O_5 (average 0.18%) and higher SiO_2 (average 76.85%), MgO (average 0.23%), CaO (average 0.64%), and FeO (average 2.44%) content to the fresh rock. Silicification are enriched in elements W (average 1370 $\times 10^{-6}$) to the fresh samples, yet gradually depleted in Nb (average 11.74 $\times 10^{-6}$), and Ta (average 4.46 $\times 10^{-6}$) (Table S1). It confirms the enrichment of element W to mineralization by hydrothermal alteration.

5. Discussion

5.1. Mass balance calculation of alteration systems

Mass balance calculation provides an important and useful method to understand the geological process, especially the absolute mass gain/loss of elements in hydrothermal systems (Zhang Y et al., 2018a). Gresens RL (1967) was first reported the idea modelling of mobility/immobility in a system, and the immobile element approaches were developed by Maclean WH (Maclean WH et al., 1987; Maclean WH, 1988, 1990). Choosing an accurate immobile element is difficult (Zhang Y et al., 2018a), therefore, in this study, the binary correlation plots by Klammer (Klammer D, 1997) to determine the immobile elements during the hydrothermal alteration at the Dahutang tungsten deposit, which is used to choose the immobile elements (Table S1). In this study, the authors had chosen the TiO_2, Ni, V, Sc, Lu, and Co as the immobile elements.

The main advantages of the graphical methods are their rapid implementation and the clarity of the diagrams (Durand C et al., 2015). The isocon method of Grant JA (1986) was used to demonstrate potential chemical changes between altered wall rocks and their corresponding "protoliths/unaltered rocks". Therefore, in this study a user-friendly interactive Microsoft Excel spreadsheet program by López-Moro (López-Moro FJ, 2012) was chosen.

All the calculations follow Grant's approach (Grant JA, 1986):

$$\Delta C = \left(C_i^{\mathrm{F}}/C_i^{\mathrm{A}}\right)\cdot C^{\mathrm{A}} - C^{\mathrm{F}}$$

where C^{F} and C^{A} are the concentrations in the fresh (F) and altered (A) sample, respectively; ΔC denotes the gain or loss in grams per 100 g of rock for major elements or in parts per million for trace elements; and "i" is the immobile element (Zhang Y et al., 2018a). The results are presented in Table 1.

Samples with sodic, and potassic alterations samples exhibited strongly depleted SiO_2 and W; while bits of reduce in Nb, and Ta, the compounds of Al_2O_3, MgO, Fe_2O_3, CaO, Na_2O, and P_2O_5 increased (see Table 1). It indicates that a large number of Si, W and some Nb, Ta migrated into the fluid system (Table 1; Fig. 5). Distinctively, the silicification sample shows strong diminution on Al_2O_3, Na_2O, K_2O, P_2O_5, Nb, and Ta, but an obvious increase of W ($\Delta C_i = 352.12 \times 10^{-6}$) (see Table 1). Silicified samples are the only ones that gained a large amount of W among the four alteration processes.

The elements Mg, Ca, and Sr exhibited strong mobility ($\Delta C_i/C_0 > 1.0$) into the sodic, potassic and greisenization alteration rock during the alkaline alteration process. Especially, the elements of Nb, Ta, and W exhibited strong mobility ($-1 < \Delta C_i/C_0 < -0.5$), and moved to the fluid from the alkaline altered rock. The elements of Al, Na, K, P and Fe^{3+} exhibited moderate mobility ($1.0 > \Delta C_i/C_0 > 0.1$ or $-0.5 < \Delta C_i/C_0 < -0.1$) (Table 1; Fig. 4), which was confirmed by the formation of a secondary albite/K-feldspar/muscovite. While the elements Mg and Sr exhibited strong mobility ($\Delta C_i/C_0 > 1.0$), Ca and W exhibited moderate mobility ($1.0 > \Delta C_i/C_0 > 0.5$), those elements are deposited from the ore-forming fluid into the silicification rock. While the Nb and Ta present strong mobility ($-1 < \Delta C_i/C_0 < -0.5$), migrated out of the porphyritic biotite granite into the hydrothermal fluid during the silicification alteration process. Yet the elements Si, Al, Na, K, P and Fe^{3+} ions, exhibited moderate mobility ($1.0 > \Delta C_i/C_0 > 0.1$) which was confirmed by the formation of a secondary muscovite, wolframite, and sulphides (Table 1).

Samples with sodic alteration lost a large quantity of W during the alteration process; as a result, they have the lowest content compared to the samples with potassic alteration and greisenization. This is due to the K_2O loss into the fluid, while

Table 1. Selected elements mass change (Gain/Loss) of the altered porphyritic biotite granite in the Dahutang tungsten deposit.

Alteration type	Strongly potassic (K-feldspar)			Strongly sodic (perthites ± albite)			Greisenization (muscovite ± quartz)			Strongly silicification (quartz ± muscovite)		
	arith.mean (2)	$\Delta C_i/C_i^0$	ΔC_i	arith.mean (2)	$\Delta C_i/C_i^0$	ΔC_i	arith.mean (5)	$\Delta C_i/C_i^0$	ΔC_i	arith.mean (3)	$\Delta C_i/C_i^0$	ΔC_i
Major oxides /%												
SiO_2	66.00	–0.09	–6.43	65.48	–0.10	–7.32	71.75	–0.01	–0.43	76.85	0.06	4.42
Al_2O_3	18.23	0.25	3.64	19.06	0.30	4.36	14.22	–0.02	–0.34	12.03	–0.18	–2.59
Fe_2O_3	0.68	0.77	0.30	0.41	0.05	0.02	0.53	0.40	0.15	0.38	0.00	0.00
MgO	0.81	2.91	0.60	0.44	1.10	0.23	0.42	1.04	0.21	0.23	0.13	0.03
CaO	1.20	1.07	0.62	1.24	1.11	0.65	1.05	0.81	0.47	0.64	0.11	0.06
Na_2O	0.25	–0.93	–3.57	6.93	0.81	3.09	1.83	–0.52	–1.98	3.08	–0.19	–0.74
K_2O	5.98	0.26	1.23	2.42	–0.49	–2.36	5.03	0.06	0.29	3.25	–0.32	–1.51
P_2O_5	0.82	1.99	0.55	0.46	0.68	0.19	0.23	–0.16	–0.04	0.18	–0.35	–0.10
LOI	2.53	3.62	1.99	1.13	1.04	0.57	1.29	1.36	0.75	0.60	0.10	0.06
FeO	3.02	0.60	1.14	2.02	0.06	0.12	3.12	0.66	1.25	2.44	0.30	0.56
Trace elements/10^{-6}												
Sr	64.7	1.02	32.86	138	3.31	106.14	88.8	1.79	57.3	26.1	–0.18	–5.85
Nb	19.9	–0.06	–1.39	13.8	–0.36	–7.59	12.7	–0.40	–8.60	11.7	–0.45	–9.58
Ta	10.8	–0.19	–2.58	4.35	–0.68	–9.08	1.77	–0.87	–11.6	4.46	–0.67	–8.94
W	130	–0.87	–891	21.1	–0.98	–1001	325	–0.68	–694	1370	0.34	352

*ΔC_i and $\Delta C_i/C_i^0$ Calculated using the excel program from López-Moro FJ, 2012; LOI means ignition loss; the "Arith. mean (2)" means average value, and the number in brackets mean the number of analyses.

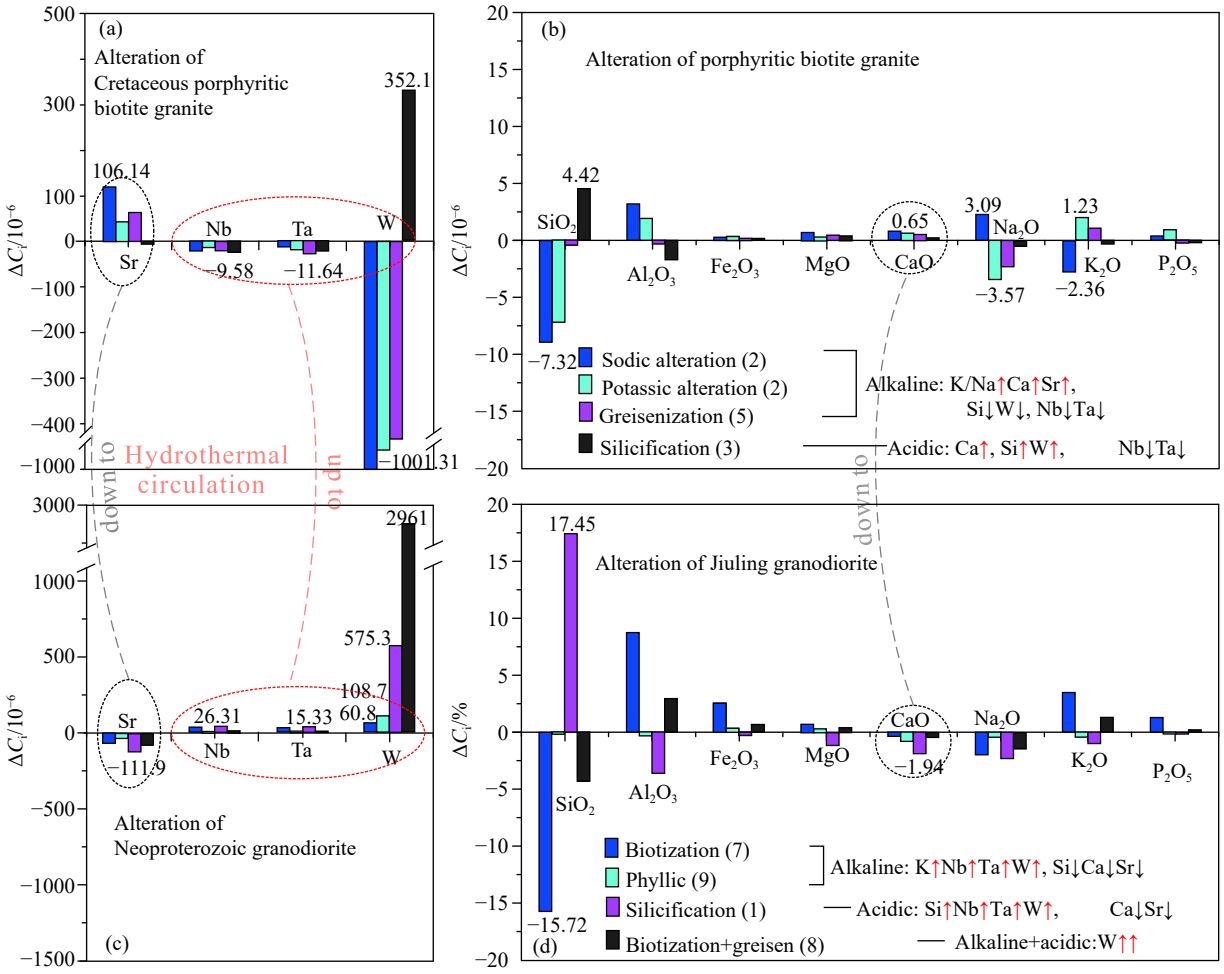

Fig. 5. Selected elements mass-change calculations of four types of alteration in the Dahutang deposit. a–trace elements of altered porphyritic biotite granite; b–major elements of altered porphyritic biotite granite; c–trace elements of altered Jiuling granodiorite (data from Zhang Y et al., 2018a, 2018b); d–major elements of altered Jiuling granodiorite (data from Zhang Y et al., 2018a, 2018b).

the solubility of the K_2WO_4 (76.05% by weight, 18℃) was almost twice that of the Na_2WO_4 (42.59% by weight, 25℃) (Liu YJ and Ma DS, 1987); thus, an enriched K fluid can leach substantial quantities of element W from the porphyritic biotite granite more than an enriched Na fluid. Therefore, sodic alteration samples can lose quantity of element W more than the potassic alteration and greisenization.

The elements of Al, Mg, Ca, P, and Fe^{3+} ions transferred into the sodic, potassic altered rock and a large quantity of Si, K, and W transferred out, which indicates an oxidized high-temperature alkaline solution, in elevation from 764.16–1369.4 m in the Dahutang deposit. The elements Al, Fe, Mg, Ca, K, and P also mobilized into the altered rock to form a large number of K-feldspar and apatite as storage on the downside (deep), released later by acidic alteration, changing to form quartz, and transferred to the upside to form wolframite and scheelite in the altered rock (Table 1; Fig. 5). A large number of Nb, Ta, and W were leached out from the porphyritic biotite granite and migrated into the fluid.

However, Si, Mg, Ca, and Fe^{2+} were transferred into the silicified rock, but the Fe^{3+}, Al, K, and P were leached out, which indicated a lower oxygen fugacity and high-temperature acidic solution. High oxygen fugacity during the alkaline alteration processes is a disadvantage for wolframite deposition. Lower oxygen fugacity during the greisenization favours deposition, which corresponds to the oxygen fugacity variation recorded in the apatite of the granite of the Dahutang tungsten deposit (Han L et al., 2016).

The elements Al, Mg, Ca, Na, P, and Sr were transferred in, but Si, Nb, Ta and W were transferred out from the porphyritic biotite granite during the sodic, potassic and greisenization alteration processes. Whereas, the elements of Si, Mg, Ca, Sr W and Fe^{2+}, migrated in, while Al, Na, K, P, Nb, and Ta migrated out of the porphyritic biotite granite during the greisenization process. The elements of Ti, Mn, Ni, V, Sc, and Lu exhibited weak mobility (immobile) during all four alteration processes.

5.2. Relationships between hydrothermal circulation and tungsten mineralization

Transport elements are subject to gain/loss by volatile/liquid components of the hydrothermal alteration, which are responsible for alteration and mineralization processes. For example, the alteration of biotite to muscovite/quartz in granite can release a mass of elements such as Sn and W (Barsukov VL, 1957; Shcherba GN, 1970; Taylor RG, 1979; Pirajno F, 1982; Eugster HP, 1985; Lentz D, 1992; Neves LJPF, 1997; Yang P and Rivers T, 2000; Chen YW et al., 2010; Li J et al., 2015) and also major elements such as Fe and Mn. The alteration of plagioclase, which is enriched in Li, Rb, Cs, Sr, Ba, Pb and REE (González-Acebrón L et al., 2012; Sun CG et al., 2017; Bédard JH, 2006), can release not only ore-forming elements but also major elements such as Ca and Na (Oliver NHS et al., 2004; Parsons I et al., 2009; Hu SX et al., 2004; Sun CG et al., 2017). It was done effectively by the superposition of alkaline alteration by acidic alteration, as the most important natural geologic process. This is especially important for scheelite and wolframite mineralization in the Dahutang to form a giant tungsten deposit. It is a new perspective for the granite-related tungsten deposit exploration.

5.2.1. The role of alkaline hydrothermal alteration on W enrichment and precipitation

Alkaline hydrothermal alteration commonly occurs in the deep parts of granite related W-Sn deposits, such as the foot floor of the “Five floor” model of vein-type tungsten deposits in the Nanling region (Liu XC et al., 2017b; Wang JC et al., 2008a; Hu SX et al., 2004). Characteristics of tungsten content in alkaline alteration shows that much less than the unaltered granite, it forms a zonation of low tungsten content (Hu SX et al., 2004). The Dahutang tungsten deposits, which are more likely the vein-type tungsten deposits in the Nanling, alkaline hydrothermal alteration commonly occurs at the foot floor of the vein-type tungsten deposits, and the porphyritic biotite granite of the Dahutang tungsten deposits (Zhang Y et al., 2020a). The element loss/gain from the altered porphyritic biotite granite reveals an alkaline alteration zonation of low tungsten content. This low tungsten zonation may be caused by the hydrothermal extracts of tungsten from wall rock.

The unaltered porphyritic biotite granite is characteristically enriched in Nb (21.4×10^{-6}), Ta (13.4×10^{-6}) and W (1020×10^{-6}), but lower in CaO (0.58%) and Sr (32.1×10^{-6}) at the Dahutang tungsten deposit. The alkaline alteration of the porphyritic biotite granite at deep level underground leach Nb, Ta, and W out during post-magmatic stage. In particular, during the sodic alteration, the fluids leach Nb about 7.59×10^{-6}, Ta about 9.08×10^{-6}, and W about 1000×10^{-6} to form a more W-enriched ore-forming fluid (Fig. 5a, b).

The unaltered Jiuling biotite granodiorite is enriched in CaO (2.24%) and Sr (121×10^{-6}), but lower in Nb (11.0×10^{-6}), Ta (1.45×10^{-6}), and W (9.65×10^{-6}) (Zhang Y et al., 2018a). The shallow alkaline alteration process of the Jiuling biotite granodiorite, such as the biotization and phyllic alteration leaches Si, Ca, and Sr out to the hydrothermal fluid (Zhang Y et al., 2018a, 2018b; Figs. 5b–d). This alkaline alteration process can make the K- and Fe-rich fluid more enriched in Ca and Sr, and might migrate deeper to the the porphyritic biotite granite, and mix with the post-magmatic hydrothermal to form the deep alkaline alterations, possibly as a storage of Ca in the form of apatite and albite (Fig. 6; Zhang Y et al., 2018a).

The *in-situ* trace element geochemical characteristics of Nb, Ta, Mo, and Sr in scheelite from Dahutang W deposit record the evolution of ore-forming fluid from early magmatic hydrothermal fluid to late mixing fluid with input of meteoric water (Zhang Y, 2018, 2020b). The mineralogy and trace element characteristics of scheelite in veinlet disseminated tungsten mineralization displays zoning texture and show two generations. The early generation has magmatic hydrothermal characteristics of higher Nb, Ta and Mo, but low Sr (44×10^{-6} to 95×10^{-6}) (Zhang Y et al., 2020b). In contrast, the scheelite at the Xi’an W deposit has low Nb, Ta and Mo, but high Sr (582×10^{-6} to 861×10^{-6}) and is possibly originated from a metamorphic fluid (Zhang Y et al., 2020b). The composition

of the late generation of scheelite from Dahutang is between early generation of Dahutang to Xi'an W deposit. The mineral chemistry characteristics of scheelite indicates that ore-forming fluids of Dahutang is dominant by magmatic hydrothermal fluid in the early stage and have addition of meteoric water during fluid evolvement (Zhang Y et al., 2020b).

Those results correspond to the chemical zoning of muscovite (Li-micas) at the Dahutang W deposit. The Li-micas not only traces the processes of W enrichment by magmatic differentiation and volatiles but also traces the leaching of W by the fluids at the Dahutang W deposit (Yin R et al., 2019). The late-stage, high-temperature, water-rich, high $\delta^{18}O$, alkalimetal-rich, low oxygen fugacity, and acidic nature of the hydrothermal fluids that formed the Dahutang deposit promoted the transportation and further deposition of tungsten (Zhang ZY et al., 2019). In addition, the Li isotopic data (Chen B et al., 2018), which suggest that the extensive tungsten mineralization accompanying the evolved granites may not only be derived from significant fluid exsolution from the granite itself as traditionally thought, but rather, from the activity of coeval metamorphic fluids and/or high temperature circulating meteoric originating fluids.

Therefore, the genetics of the Dahutang tungsten deposit may not concur with traditional thought. It is mainly a magmatic fluid enriched in W and had experienced a fluid circulation to extract much of the W from the porphyritic biotite granite through fluid-rock reactions. The four types of altered wall rock at the Dahutang tungsten deposit recorded all the evolution process.

5.2.2. Hydrothermal circulation and superimposed alteration events

For the superimposed alteration events, alkaline-by-acidic controls the regional distribution of the main alteration types at the Dahutang tungsten deposit. The alkaline and acidic alteration might correspond to two magmatic events (Zhang Y et al., 2018a), the porphyritic biotite granite (about 150 Ma; Zhang MY et al., 2016a) and fine-grained biotite granite (about 144 Ma; Mao ZH et al., 2015; Fig. 3). The hydrothermal circulation and superimposed alteration process may be as follows.

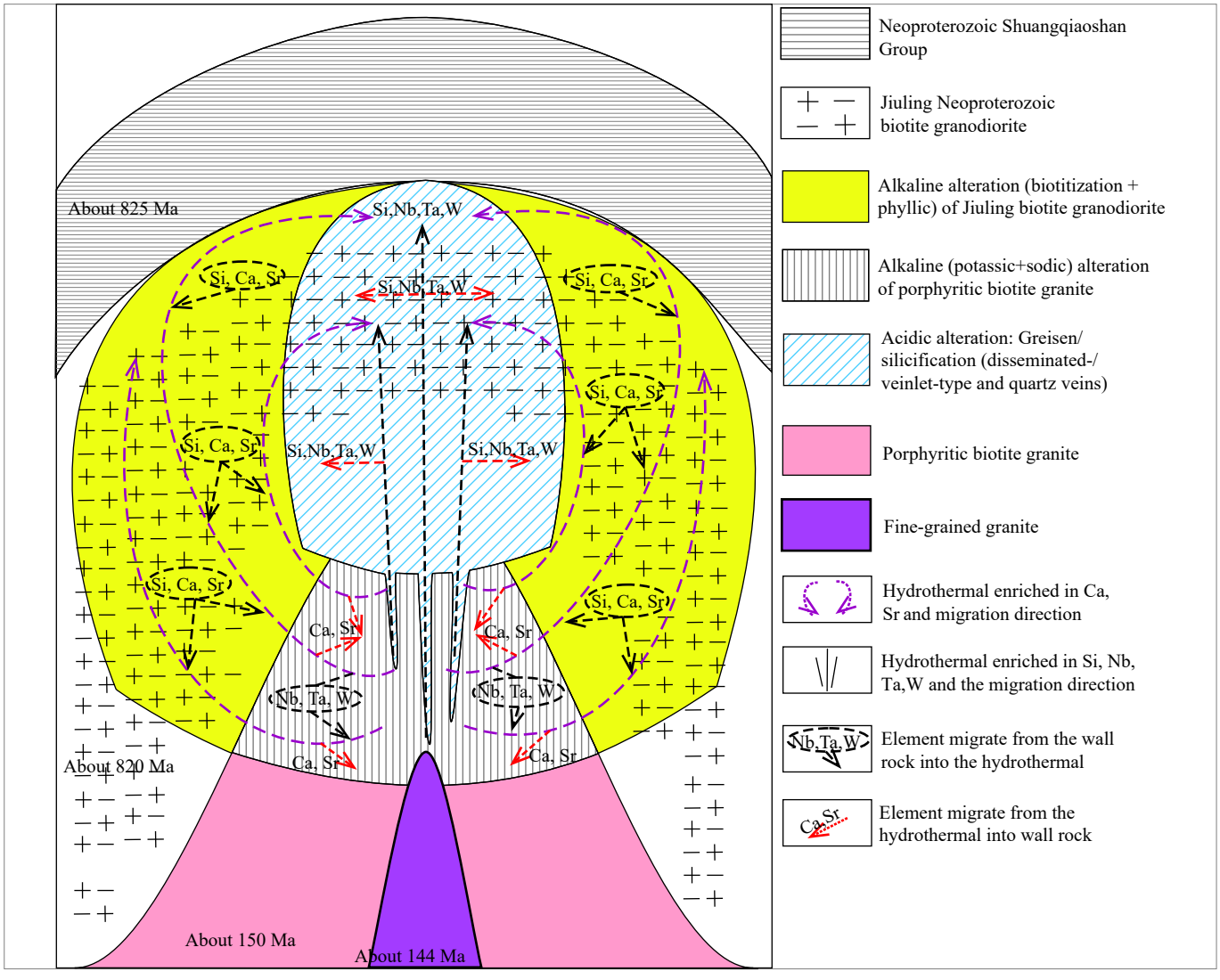

Fig. 6. Hydrothermal circulation model in the Dahutang tungsten deposit.

The deep alkaline alterations (albitization, potassic alteration and greisenization) leaches the Nb, Ta, and W from the porphyritic biotite granite, especially during the sodic alteration process (Table 1; Fig. 5a). This alkaline alteration process can make the fluid more enriched in K, Fe, Nb, Ta, and W, and migrate to the upside (the Jiuling biotite granodiorite), to form another most important alteration, the biotization (Fig. 6), As a result, a massive hydrothermal biotite presents as a storage of Fe and W (Zhang Y et al., 2018a).

Simultaneously, the upper alkaline alteration that leached Si, Ca and Sr from the biotite granodiorite into the fluid (Zhang Y et al., 2018a, 2018b), generated the hydrothermal fluid enriched in Si, W and Sr, and circuited down to the deep side, the porphyritic biotite granite, and converged with the magmatic fluid, to form the greisenization (Fig. 6).

Finally, the alkaline hydrothermal fluid ’s pH might become acidic, probably due to K and Na consumption by fluid/rock activity and possibly associated with the acidic fluid from the fine-grained biotite granite (about 144 Ma) magmatic (Fig. 6). This acidic ore-forming fluid migrated to the upper biotization rock. In addition, the elements of Si, W and Sr deposit, to form wolframite, scheelite, and quartz, respectively after fluid/rock action. During acidic (silicification) alteration, the biotite changes to muscovite and can release significant quantities of Fe-Mn and some W to form wolframite. The fluid that has insufficient Ca forms a single scheelite deposit, because of the large quantities of Fe and Mn released from the alteration of biotite to muscovite/quartz. The result is the formation of a scheelite/wolframite (about 1) deposit (Fig. 6).

This hydrothermal circulation model of the Dahutang tungsten deposit offers a deeper understanding of the element behaviour in alteration processes and tungsten mineralization.

6. Conclusion

The elements of Ti, Mn, Ni, V, Sc, and Lu exhibited immobility during all four-alteration processes. The albitization of porphyritic biotite results in Mg, Ca, Na, P, and Sr gain, and Si, K, Nb, Ta, and W loss. However, the Fe^{3+} and Fe^{2+} ions exhibited immobile. The potassic alteration of porphyritic biotite granite is characterized by Fe^{3+}, Mg, Ca, P, and Sr gain, and Si, Na, Nb, Ta, and W loss. The greisenization of porphyritic biotite granite is featured by Fe^{3+}, Mg, Ca, K, and Sr gain, and Si, Na, Nb, Ta, and W loss, and immobility of P. The silicification of porphyritic biotite granite has characteristics of Si, Mg, Ca, Fe^{2+}, Sr and W gain, and Na, K, P, Nb and Ta loss.

The fresh porphyritic biotite granite has high Nb, Ta, and W, but low Ca and Sr contents, while the Jiuling granodiorite have high Ca and Sr, but low Nb, Ta, and W contents. The altered porphyritic biotite granite indicated that the Nb, Ta, and W, leached out from the fresh porphyritic biotite granite, especially by sodic alteration. The low Ca and Sr contents of the altered Neoproterozoic Jiuling granodiorite indicate that Ca and Sr had been leached out from the fresh granodiorite by the fluid around Mesozoic porphyritic biotite.

CRediT authorship contribution statement

Yong Zhang conceived of the presented idea. Hai-Bo Zhao wrote the manuscript with support from Yong Zhang. Yong Zhang developed the theoretical formalism. Both Hai-Bo Zhao and Lei Liu contributed to the final version of the manuscript.

Declaration of competing interest

The authors declare no conflicts of interest.

Acknowledgment

The authors would like to thank Mr. Xin-kui Xiang, Mr. Lan-qing Liu and their co-workers from the Jiangxi Bureau of Geology, Mineral Resources, Exploration and Development, and its affiliated No. 916 Geological Team and Northwestern Geological Team, for field guidance and constructive discussions, and additionally to the reviewers ’ constructive comments on this manuscript. Thanks to the Analytical Laboratory Beijing Research Institute of Uranium Geology for completing the analysis and testing of major/trace elements of the bulk rock. This research is jointly funded by the Project of China Geological Survey (DD20190186 and 12120114034501) and National Natural Science Foundation of China (42062006 and 41962007). The authors would like to thank the two reviewers and editors very much for their constructive comments.

Appendix data

Supplementary data (Table S1) to this article can be found online at doi: 10.31035/cg2021003.

References

Bédard JH. 2006. Trace element partitioning in plagioclase feldspar. Geochimica et Cosmochimica Acta, 70(14), 3717–3742. doi: 10.1016/j.gca.2006.05.003.

Barsukov VL. 1957. The geochemistry of tin. Geokimiya, 1, 41–53.

Chen B, Gu H-o, Chen Y, Sun K, Chen W. 2018. Lithium isotope behaviour during partial melting of metapelites from the Jiangnan Orogen, South China: Implications for the origin of REE tetrad effect of F-rich granite and associated rare-metal mineralization. Chemical Geology, 483, 372–384. doi: 10.1016/j.chemgeo.2018.03.002.

Chen GH, Wan HZ, Shu LS. 2012. An analysis on ore-controlling conditions and geological features of the Cu-W polymetallic ore deposit in the Zhuxi area of Jingdezhen, Jiangxi Province. Acta Petrologica Sinica, 28(12), 3901–3914 (in Chinese with English abstract). doi: 10.1134/S0869593812070027.

Chen YW, Bi XW, Hu RZ, Zhu WG, Xu LL, Dong SH. 2010. The geochemical characteristics of biotites and their constraints on uranium mineralization in guidong pluton. Bulletin of Mineralogy Petrology & Geochemistry, 29(4), 355–363 (in Chinese with English abstract). doi: 10.3724/SP.J.1231.2010.06586.

Cooke DR. 2005. Giant porphyry deposits: Characteristics, distribution, tectonic controls. Economic Geology, 100(5), 801–818. doi: 10.2113/gsecongeo.100.5.801.

Cooke DR, Hollings P, Wilkinson JJ, Tosdal, RM. 2014. 13.14-

Geochemistry of porphyry deposits. Treatise on Geochemistry, 1(3), 357–381.
Corbett GJ, Leach TM. 1998. Southwest Pacific Rim gold-copper systems: structure, alteration and mineralisation. Society of Economic Geologists, 237 pp.
Ding X, Jiang SY, Ni P, Gu LX, Jiang YH. 2005. Zircon SIMS U-Pb geochronology of host granitoids in Wushan and Yongping copper deposits, Jiangxi Province. Geological Journal of China Universities, 11(3), 383–389 (in Chinese with English abstract).
Durand C, Oliot E, Marquer D, Sizun JP. 2015. Chemical mass transfer in shear zones and metacarbonate xenoliths: A comparison of four mass balance approaches. European Journal of Mineralogy, 27, 731–754. doi: 10.1127/ejm/2015/0027-2475.
Eugster HP. 1985. Granites and hydrothermal ore deposits: A geochemical framework. Mineralogical Magazine, 49(350), 7–23. doi: 10.1180/minmag.1985.049.350.02.
Feng CY, Zhang DQ, Xiang XK, Li DX, Qu HY, Liu JN, Xiao Y. 2012. Re-Os isotopic dating of molybdenite from the Dahutang tungsten deposit in northwestern Jiangxi Province and its geological implication. Acta Geologica Sinica, 28(12), 3858–3868 (in Chinese with English abstract).
Gao JF, Lu JJ, Lai MY, Lin YP, Pu W. 2003. Analysis of Trace Elements in Rock Samples Using HR-ICPMS. Journal of Nanjing University, 39(6), 844–850 (in Chinese with English abstract).
González-Acebrón L, Götze J, Barca D, Arribas J, Mas R, Pérez-Garrido C. 2012. Diagenetic albitization in the Tera Group, Cameros Basin (NE Spain) recorded by trace elements and spectral cathodoluminescence. Chemical Geology, 312–313, 148–162. doi: 10.1016/j.chemgeo.2012.04.012.
Grant JA. 1986. The isocon diagram-A simple solution to Gresens' equation for Metasomatic alteration. Economic Geology, 81(8), 1976–1982. doi: 10.2113/gsecongeo.81.8.1976.
Gresens RL. 1967. Composition-volume relationships of metasomatism. Chemical Geology, 2(67), 47–65. doi: 10.1016/0009-2541(67)90004-6.
Gustafson LB, Hunt JP. 1975. The porphyry copper deposit at El Salvador, Chile. Economic Geology, 70(5), 857–912. doi: 10.2113/gsecongeo.70.5.857.
Han L, Huang X, Li J, He P, Yao J. 2016. Oxygen fugacity variation recorded in apatite of the granite in the Dahutang tungsten deposit, Jiangxi Province, South China. Acta Petrologica Sinica, 32(3), 746–758 (in Chinese with English abstract).
Harris AC, Golding SD. 2002. New evidence of magmatic-fluid related phyllic alteration: Implications for the genesis of porphyry Cu deposits. Geology, 30(4), 335–338. doi: 10.1130/0091-7613(2002)0302.0.CO;2.
Hou ZQ, Pan XF, Yang ZM, Qu XM. 2007. Porphyry Cu-(Mo-Au) deposits no related to oceanic-slab subduction: Examples from Chinese porphyry deposits in continental settings. Geoscience, 21(2), 332–351 (in Chinese with English abstract).
Hou ZQ, Zheng YC, Yang ZM, Yang ZS. 2012. Metallogenesis of continental collision setting: Part I, Gangdese Cenozoic porphy Cu-Mo systems in Tibet. Mineral Deposits, 31(4), 647–670 (in Chinese with English abstract).
Hu SX, Ye Y, Fang CQ. 2004. Petrology of Metasomatic Rocks and Implieations Fur Ore Exploration. Beijing, Geological publishing house, 109. (in Chinese).
Hu ZH, Liu D, Liu SB, Lang XH, Zhang JJ, Chen YC, Shi GH, Wang YY, Lei TH, Nei LM, Sha M, Gong LX, Liu ZQ. 2015. Rock-forming and ore-forming ages and significance of Taqian Mo (W) deposit, Leping, Jiangxi, China. Journal of Chengdu University of Technology, 42(3), 312–322 (in Chinese with English abstract). doi: 10.3969/j.issn.1671-9727.2015.03.07.
Huang LC, Jiang SY. 2013. Geochronology, geochemistry and petrogenesis of the tungsten-bearing porphyritic granite in the Dahutang tungsten deposit, Jiangxi Province. Acta Petrologica Sinica, 29(12), 4323–4335 (in Chinese with English abstract).
Huang LC, Jiang SY. 2014. Highly fractionated S-type granites from the giant Dahutang tungsten deposit in Jiangnan Orogen, Southeast China: Geochronology, petrogenesis and their relationship with W-mineralization. Lithos, 202(4), 207–226. doi: 10.1016/j.lithos.2014.05.030.
Jia LQ, Xu WY, Yang D, Yang ZS, Mo XX, Wang L. 2015a. Zircon U-Pb and molybdenite Re-Os dating of the Dongleiwan skarn Cu polymetallic deposit in Jiangxi Province, Eastern China. Acta Geologica Sinica, 36(2), 177–186 (in Chinese with English abstract).
Jia LQ, Xu WY, Yang D, Yang ZS, Wang L. 2015b. Zircon U-Pb and molybdenite Re-Os dating of Baoshan porphyry Cu polymetallic deposit in Jiujiang-Ruichang ore concentration area of Jiangxi Province and its geological significance. Mineral Deposits, 34(1), 63–80 (in Chinese with English abstract). doi: 10.1007/s11442-008-0201-7.
Jiang SY, Peng NJ, Huang LC, Xu YM, Zhan GL, Dan XH. 2015. Geological characteristic and ore genesis of the giant tungsten deposits from the Dahutang ore-concentrated district in northern Jiangxi Province. Acta Petrologica Sinica, 31(3), 639–655 (in Chinese with English abstract).
Klammer D. 1997. Mass change during extreme acid-sulphate hydrothermal alteration of a Tertiary latite, Styria, Austria. Chemical Geology, 141(1−2), 33–48. doi: 10.1016/S0009-2541(97)00056-9.0.
Kusakabe M. 1984. Oxygen and sulfur isotopic compositions of quartz, an hydrite and sulfide minerals from the El Teniente and Rio Blanco porphyry copper deposits, Chile. Bulletin of the Geological Survey of Japan, 35, 583–614.
Kusakabe M, Hori M, Matsuhisa Y. 1990. Primary mineralization-alteration of the El Teniente and Río Blanco porphyry copper deposits, Chile: Stable isotope, fluid inclusion and $Mg^{+2}/Fe^{+2}/Fe^{+3}$ ratios of hydrothermal fluids. In: Herbert HK, Ho SE (eds.) Stable isotopes and fluid processes in mineralization. University of Western Australia Press, Perth, 244–259.
López-Moro FJ. 2012. EASYGRESGRANT —A Microsoft Excel spreadsheet to quantify volume changes and to perform mass-balance modeling in metasomatic systems. Computers & Geosciences, 39, 191–196. doi: 10.1016/j.cageo.2011.07.014.
Lecumberri-Sanchez P, Vieira R, Heinrich CA, Pinto F, W?lle M. 2017. Fluid-rock interaction is decisive for the formation of tungsten deposits. Geology, 45(7), 579–582. doi: 10.1130/G38974.1.
Lentz D. 1992. Petrogenesis and geochemical composition of biotites in rare-element granitic pegmatites in the southwestern Grenville Province, Canada. Mineralogy and Petrology, 46(3), 239–256. doi: 10.1007/BF01164649.
Li J, Huang XL, He PL, Li WX, Yu Y, Chen LL. 2015. In situ analyses of micas in the Yashan granite, South China: Constraints on magmatic and hydrothermal evolutions of W and Ta-Nb bearing granites. Ore Geology Reviews, 65, 793–810. doi: 10.1016/j.oregeorev.2014.09.028.
Li XH, Li ZX, Ge W, Zhou H, Li W, Liu Y, Wingate MTD. 2003. Neoproterozoic granitoids in South China: Crustal melting above a mantle plume at about 825 Ma? Precambrian Research, 122(s1–4), 45–83. doi: 10.1016/S0301-9268(02)00207-3.
Li Y, Pan XF, Zhao M, Chen GH, Zhang TF, Liu X, Zhang C. 2014. LA-ICP-MS zircon U-Pb age, geochemical features and relations to the W-Cu mineralization of granitic porphyry in Zhuxi skarn deposit, Jingdezhen, Jiangxi. Geological Review, 60(3), 693–708 (in Chinese with English abstract).
Liang Q, Grégoire DC. 2000. Determination of trace elements in twenty six Chinese geochemistry reference materials by inductively coupled plasma−Mass Spectrometry. Geostandards & Geoanalytical Research, 24(1), 51–63 (in Chinese with English abstract). doi: 10.1111/j.1751-908X.2000.tb00586.x.
Liu J, Mao JW, Ye HS, Xie GQ, Yang GQ, Zhang W. 2008. Zircon LA-ICPMS U-Pb dating of Hukeng granite in Wugongshan area, Jiangxi Province and its geoehemical characteristics. Acta Petrologica Sinica, 24(8), 1813–1822 (in Chinese with English abstract).
Liu JX, Chen HW, Liu XC, Wang G, Chao LI, Zhang JG. 2015. Isotopic age dating of Huashandong tungsten deposit in Xiushui County, Jiangxi Province and its geological significance. Resources Survey & Environment, 36(1), 1–9 (in Chinese with English abstract).
Liu SB, Liu ZQ, Wang CH, Wang DH, Zhao Z, Hu ZH. 2017a. Geochemical characteristics of REEs and trace elements and Sm-Nd

dating of scheelite from the Zhuxi giant tungsten deposit in northeast Jiangxi. Earth Science Frontiers, 24(5), 17–30 (in Chinese with English abstract). doi: 10.13745/j.esf.yx.2017-1-3.

Liu XC, Zhang DH, Zhao B, Liao ZZ, Liu CP. 2017b. Quantitative analysis of the "Five-floor" vertical morphological zonation in the Piaotang tungsten deposits, South China. Geological Journal of China Universities, 23(3), 408–416 (in Chinese with English abstract).

Liu YJ, Ma DS. 1987. Geochemistry of tungsten. Beijing, Science Press, 1–232. (in Chinese).

Liu YY, Ma CQ, Zhao Y, Huang WP. 2012. Zircon U-Pb age, element and Sr-Nd-Hf isotope geochemistry of Late Mesozoic magmatism from the Guichi metallogenic district in the Middle and Lower Reaches of the Yangtze River Region. Acta Petrologica Sinica, 28(10), 3287–3305 (in Chinese with English abstract).

Lou FS, Shen WZ, Wang DZ, Shu LS, Wu FJ, Zhang FR, Yu JH. 2005. Zircon U-Pb isotopic chronology of the Wugongshan dome compound granite in Jiangxi Province. Acta Geologica Siniabout, 79(5), 637–644 (in Chinese with English abstract).

Lowell JD, Guilbert JM. 1970. Lateral and vertical alteration-mineralization zoning in porphyry ore deposits. Economic Geology, 65(4), 373–408. doi: 10.2113/gsecongeo.65.4.373.

Maclean WH. 1988. Rare earth element mobility at constant inter-REE ratios in the alteration zone at the Phelps Dodge massive sulphide deposit, Matagami, Quebec. Mineralium Deposita, 23(4), 231–238. doi: 10.1007/BF00206399.

Maclean WH. 1990. Mass change calculations in altered rock series. Mineralium Deposita, 25(1), 44–49. doi: 10.1007/BF03326382.

Maclean WH, Kranidiotis P, Maclean WH, Kranidiotis P. 1987. Immobile elements as monitors of mass transfers in hydrothermal alteration: Phelps Dodge massive sulfide deposit, Matagami, Quebec. Economic Geology, 82(4), 951–962. doi: 10.2113/gsecongeo.82.4.951.

Mao JW, Guy B, Raimbault L, Shimazaki H. 1996. Manganese skarn in the Shizhuyuan polymetallic tungsten deposit, Hunan, China. Resource Geology, 46(1), 1–11.

Mao JW, Wang YT, Lehmann B, Yu JJ, Du AD, Mei YX, Li YF, Zang WS, Stein HJ, Zhou TF. 2006. Molybdenite Re-Os and albite $^{40}Ar/^{39}Ar$ dating of Cu-Au-Mo and magnetite porphyry systems in the Yangtze River valley and metallogenic implications. Ore Geology Reviews, 29(3–4), 307–324. doi: 10.1016/j.oregeorev.2005.11.001.

Mao JW, Xie GY, Chao D, Franco P, Dazio I, Chen YC. 2011. A tectono-genetic model for porphyry-skarn-stratabound Cu-Au-Mo-Fe and magnetite-apatite deposits along the Middle-Lower Yangtze River Valley, Eastern China. Ore Geology Reviews, 43(1), 294–314. doi: 10.1016/j.oregeorev.2011.07.010.

Mao ZH, Cheng YB, Liu JJ, Yuan SD, Wu SH, Xiang XK, Luo XH. 2013. Geology and molybdenite Re-Os age of the Dahutang granite-related veinlets-disseminated tungsten ore field in the Jiangxin Province, China. Ore Geology Reviews, 53, 422–433. doi: 10.1016/j.oregeorev.2013.02.005.

Mao ZH, Liu JJ, Mao JW, Deng J, Zhang F, Meng XY, Xiong BK, Xiang XK, Luo XH. 2015. Geochronology and geochemistry of granitoids related to the giant Dahutang tungsten deposit, middle Yangtze River region, China: Implications for petrogenesis, geodynamic setting, mineralization. Gondwana Research, 28(2), 816–836. doi: 10.1016/j.gr.2014.07.005.

Nadeau O. 2015. Economic geology: Ore metals beneath volcanoes. Nature Geoscience, 8(3), 168–170. doi: 10.1038/ngeo2379.

Neves LJPF. 1997. Trace element content and partitioning between biotite and muscovite of granitic rocks: A study in the Viseu region (Central Portugal). European Journal of Mineralogy, 9(4), 849–857. doi: 10.1127/ejm/9/4/0849.

Oliver NHS, Cleverley JS, Mark G, Pollard PJ, Fu B, Marshall LJ, Rubenach MJ, Williams PJ, Baker T. 2004. Modeling the role of sodic alteration in the genesis of iron oxide-copper-gold deposits, eastern mount Isa Block, Australia. Economic Geology, 99, 1145–1176. doi: 10.2113/gsecongeo.99.6.1145.

Pan YM, Dong P. 1999. The Lower Changjiang (Yangzi/Yangtze River) metallogenic belt, east central China: Intrusion- and wall rock-hosted Cu-Fe-Au, Mo, Zn, Pb, Ag deposits. Ore Geology Reviews, 15(4), 177–242. doi: 10.1016/S0169-1368(99)00022-0.

Parsons I, Magee CW, Allen CM, Shelley JMG, Lee MR. 2009. Mutual replacement reactions in alkali feldspars Ⅱ: Trace element partitioning and geothermometry. Contributions to Mineralogy and Petrology, 157(5), 663–687. doi: 10.1007/s00410-008-0358-1.

Pirajno F. 1982. Geology, geochemistry, mineralisation, metal zoning of the McConnochie greisenised granite, Reefton district, Westland, New Zealand. New Zealand. Journal of Geology & Geophysics, 25(4), 405–425. doi: 10.1080/00288306.1982.10421507.

Pirajno F. 2013. Effects of Metasomatism on Mineral Systems and Their Host Rocks: Alkali Metasomatism, Skarns, Greisens, Tourmalinites, Rodingites, Black-Wall Alteration and Listvenites, Metasomatism and the Chemical Transformation of Rock. Lecture Notes in Earth System Sciences. Berlin, Springer Berlin Heidelberg. 203–251.

Plümper O, Botan A, Los C, Liu Y, Malthesørenssen A, Jamtveit B. 2017a. Fluid-driven metamorphism of the continental crust governed by nanoscale fluid flow. Nature Geoscience, 10(9), 685–691. doi: 10.1038/ngeo3009.

Plümper O, John T, Podladchikov YY, Vrijmoed JC, Scambelluri M. 2017b. Fluid escape from subduction zones controlled by channel-forming reactive porosity. Nature Geoscience, 10(2), 150–156. doi: 10.1038/ngeo2865.

Seedorff E, Dilles JH, Proffett JM, Einaudi MT, Zurcher L, Stavast WJA, Johnson DA, Barton MD. 2005. Porphyry deposits: Characteristics and origin of hypogene features. Economic geology, 100th anniversary volume, 251–298. doi: 10.5382/AV100.10.

Shcherba GN. 1970. Greisens. International Geology Review, 12(2), 114–150. doi: 10.1080/00206817009475216.

Sial AN, Bettencourt JS, De Campos CP, Ferreira VP. 2011. Granite-related ore deposits: An introduction. Geological Society London Special Publications, 350(1), 1–5. doi: 10.1144/SP350.1.

Sillitoe RH. 1997. Characteristics and controls of the largest porphyry copper-gold and epithermal gold deposits in the circum-Pacific region. Australian Journal of Earth Sciences, 44(3), 373–388. doi: 10.1080/08120099708728318.

Sillitoe RH. 2000. Gold-rich porphyry deposits, descriptive and genetic models and their role in exploration and discovery. Seg Reviews, 13, 315–345.

Sillitoe RH. 2010. Porphyry copper systems. Economic Geology, 105(1), 3–41. doi: 10.2113/gsecongeo.105.1.3.

Soloviev SG, Kryazhev S. 2016. Geology, mineralization, fluid inclusion characteristics of the Chorukh-Dairon W-Mo-Cu skarn deposit in the Middle Tien Shan, Northern Tajikistan. Ore Geology Reviews, 80, 79–102. doi: 10.1016/j.oregeorev.2016.06.021.

Soloviev SG, Kryazhev SG. 2017. Geology, mineralization, fluid inclusion characteristics of the Skrytoe reduced-type W skarn and stockwork deposit, Sikhote-Alin, Russia. Mineralium Deposita, 52(6), 1–26. doi: 10.1007/s00126-016-0705-5.

Sun CG, Graff M, Liang Y. 2017. Trace element partitioning between plagioclase and silicate melt: The importance of temperature and plagioclase composition, with implications for terrestrial and lunar magmatism. Geochimica et Cosmochimica Acta, 206, 273–295. doi: 10.1016/j.gca.2017.03.003.

Sun KK, Chen B. 2017. Trace elements and Sr-Nd isotopes of scheelite: Implications for the W-Cu-Mo polymetallic mineralization of the Shimensi deposit, South China. American Mineralogist, 102(5), 1114–1128. doi: 10.2138/am-2017-5654.

Taylor RG. 1979. Geology of tin deposits. Elsevier Scientific Pub. Co., distributors for the U.S. and Canada, Elsevier/North-Holland, 543.

Wang H, Feng C, Zhao Y, Zhang M, Chen R, Chen J. 2016. Ore genesis of the Lunwei granite-related scheelite deposit in the Wuyi metallogenic belt, Southeast China: Constraints from geochronology, fluid inclusions, H-O-S isotopes. Resource Geology, 66(3), 240–258. doi: 10.1111/rge.12100.

Wang JC, Wei LM, Zhu WF, Wan FL. 2008a. Texture and tectonic style of "Five-storeyed Type" for the tungsten deposits in the Nanling Mountains, Southern China−An example from the Meiziwo tungsten deposit. Acta Geologica Sinica, 82(7), 894–899 (in Chinese with

English abstract).
Wang XL, Zhao GC, Zhou JC, Liu YS, Hu J. 2008b. Geochronology and Hf isotopes of zircon from volcanic rocks of the Shuangqiaoshan Group, South China: Implications for the Neoproterozoic tectonic evolution of the eastern Jiangnan orogen. Gondwana Research, 14(3), 355–367. doi: 10.1016/j.gr.2008.03.001.
Watanabe Y, Hedenquist JW. 2001. Mineralogical and stable isotope zonation at the surface over the El Salvador porphyry Cu deposit, Chile. Economic Geology, 96, 1775–1797. doi: 10.2113/96.8.1775.
Weisheit A, Bons PD, Elburg MA. 2013. Long-lived crustal-scale fluid flow: The hydrothermal mega-breccia of Hidden Valley, Mt. Painter Inlier, South Australia. International Journal of Earth Sciences, 102(5), 1219–1236. doi: 10.1007/s00531-013-0875-7.
Wolfe R, Cooke D, Hooper B, Heithersay P. 1996. A magmatic origin for late-stage sericite-alunite alteration at the Endeavour 48 Cu-Au porphyry deposit, Goonumbla, NSW, 13th Australian Geological Convention, Canberra, Australia. Earth Sciences, 480 pp.
Xiang XK, Wang P, Sun DM, Zhong B. 2013a. Re-Os isotopic age of molybdeinte from the Shimensi tungsten polymetallic deposit in northern Jiangxi province and its geological implications. Geological Bulletin of China, 32(11), 1824–1831 (in Chinese with English abstract).
Xiang XK, Wang P Zhan GN, Sun DM, Zhong B, Qian ZY, Tan R. 2013b. Geological characteristics of Shimensi tungsten polymetallic deposit in northern Jiangxi Province. Mineral Deposits, 32(6), 1171–1187 (in Chinese with English abstract).
Xiong X, Xu WY, Wen CH. 2015. Fluid characteristics and genesis of Xianglushan skam scheelite deposit in. Mineral Deposits, 34(5), 1046–1056 (in Chinese with English abstract).
Xu XB, Zhang YQ, Jia D, Shu LS, Wang, RR. 2009. Early Mesozoic geotectonic processes in South China. Geology in China, 36(3), 573–593 (in Chinese with English abstract). doi: 10.1016/S1874-8651(10)60080-4.
Yang MG, Wang FN, Zeng Y, Lai XP, Huang SB, Zhou H. 2004. Geology of Metallogenesis in Notherm Jiangxi Province. Wuhan, China Earth Press, 186. (in Chinese).
Yang P, Rivers T. 2000. Trace element partitioning between coexisting biotite and muscovite from metamorphic rocks, Western Labrador: Structural, compositional and thermal controls. Geochimica et Cosmochimica Acta, 64(8), 1451–1472. doi: 10.1016/S0016-7037(99)00425-1.
Yin R, Han L, Huang XL, Li J, Li WX, CHen LL. 2019. Textural and chemical variations of micas as indicators for tungsten mineralization: Evidence from highly evolved granites in the Dahutang tungsten deposit, South China. American Mineralogist, 104(7), 949–965. doi: 10.2138/am-2019-6796.
Zaw K, Peters SG, Cromie P, Burrett C, Hou Z. 2007. Nature, diversity of deposit types and metallogenic relations of South China. Ore Geology Reviews, 31(1), 3–47. doi: 10.1016/j.oregeorev.2005.10.006.
Zhang FX, Pointeau V, Shuller LC, Reaman DM, Lang M, Liu Z, Hu J, Panero WR, Becker U, Poinssot C, Ewing RC. 2009. Structural transitions and electron transfer in coffinite, USiO4, at high pressure. American Mineralogist, 94(7), 916–920. doi: 10.2138/am.2009.3111.
Zhang JJ, Mei YP, Wang DH, Li HQ. 2008. Isochronology study on the Xianglushan scheelite deposit in north Jiangxi Province and its geological significance. Acta Geologica Sinica, 82(7), 927–931 (in Chinese with English abstract).
Zhang MY, Feng CY, Li DX, Wang H, Zhou JH, Ye SZ, Wang GH. 2016a. Geochronological study of the Kunshan W-Mo-Cu deposit in the Dahutang area, northern Jiangxi Province and its geological significance. Geotectonica et Metallogenia, 40(3), 503–516 (in Chinese with English abstract).
Zhang Y. 2018. Ore-forming Fluid Evolution and Sb-Au-W Metallogenesis in the Central Hunan-Northwestern Jiangxi, South China. Nanjing, Najing University, 145. (in Chinese).
Zhang Y, Gao JF, Ma DS, Pan J. 2018a. The role of hydrothermal alteration in tungsten mineralization at the Dahutang tungsten deposit, South China. Ore Geology Reviews, 95, 1008–1027. doi: 10.1016/j.oregeorev.2018.04.006.
Zhang Y, Liu NQ, Pan JY, Xiang XK, Jiang QX, Jiang CQ, Jiang YY, Ding WK. 2018b. The superposition of alkaline by acidic hydrothermal alteration and its formation mechanism at Dahutang tungsten deposit, South China. Beijing, Science Press, 116. (in Chinese).
Zhang Y, Pan J, Ma D S, Liu G, Liu Y, Yang C, Zhang L. 2015a. Re‐Os molybdenite ages of Dahutang granite-related tungsten ore field, South China. Acta Geologica Sinica (English Edition), 88(s2), 1043–1044.
Zhang Y, Pan JY, Ma DS, Dan XH, Zhang LL, Xu GH, Yang CP, Jiang QX, Jiang CQ. 2017. Re-Os molybdenite age of Dawutang tungsten ore district of northwest Jiangxi and its geological significance. Mineral Deposits, 36(3), 749–769 (in Chinese with English abstract).
Zhang Y, Pan JY, Ma DS. 2020a. Lithium element enrichment and inspiration for prospecting for rare- metal mineralization in the Dahutang tungsten deposit: Constraints from mineralogy and geochemistry of hydrothermal alteration. Acta Geologica Siniabout, 94(11), 3321–3342 (in Chinese with English abstract). doi: 10.19762/j.cnki.dizhixuebao.2020218.
Zhang Y, Ma D, Gao JF. 2020b. Origin and evolution of ore-forming fluids in a tungsten mineralization system, Middle Jiangnan orogenic belt, South China: Constraints from in-situ LA-ICP-MS analyses of scheelite. Ore Geology Reviews, 127, 103806. doi: 10.1016/j.oregeorev.2020.103806.
Zhang YQ, Dong SW, Li JH, Cui JJ, Shi W, Su JB, Li Y. 2012. The new progress in the study of Mesozoic tectonics of South China. Acta Geoscientica Sinica, 33(3), 257–279 (in Chinese with English abstract). doi: 10.3975/cagsb.2012.03.01.
Zhang ZY, Hou ZQ, Peng HM, Fan XK, Wu XY, Dai JL. 2019. In situ oxygen isotope, trace element, fluid inclusion evidence for a primary magmatic fluid origin for the shell-shaped pegmatoid zone within the giant Dahutang tungsten deposit, Jiangxi Province, South China. Ore Geology Reviews, 104, 540–560. doi: 10.1016/j.oregeorev.2018.11.013.
Zhang ZY, Hou ZQ, Peng HM, Zhu XQ, Pan XF, Ye ZY. 2015b. Exsolution of primary fluids from magma in the superlarge Dahutang tungsten deposit of Jiangxi Province: Records from the pegmatoid shell. Geological Bulletin of China, 34(2), 487–500 (in Chinese with English abstract).
Zhong YF, Ma CQ, She ZB, Lin GC, Xu HJ, Wang RJ, Yang KG, Liu Q. 2005. SHRIMP U-Pb Zircon Geochronology of the Jiuling Granitic Complex Batholith in Jiangxi Province. Earth Sciences, 30(6), 685–691 (in Chinese with English abstract).